1521-009X/44/12/1881–1889$25.00
Drug Metabolism and Disposition

http://dx.doi.org/10.1124/dmd.116.071423
Drug Metab Dispos 44:1881–1889, December 2016

Brain Distribution and Efficacy of the Brain Penetrant PI3K Inhibitor GDC-0084 in Orthotopic Mouse Models of Human Glioblastoma

Laurent Salphati, Bruno Alicke, Timothy P. Heffron, Sheerin Shahidi-Latham, Merry Nishimura, Tim Cao, Richard A. Carano, Jonathan Cheong, Joan Greve, Hartmut Koeppen, Shari Lau, Leslie B. Lee, Michelle Nannini-Pepe, Jodie Pang, Emile G. Plise, Cristine Quiason, Linda Rangell, Xiaolin Zhang, Stephen E. Gould, Heidi S. Phillips, and Alan G. Olivero

Departments of Drug Metabolism and Pharmacokinetics (L.S., S.S.-L., J.C., J.P., E.G.P., C.Q., X.Z.), Discovery Chemistry (T.P.H., A.G.O.), Cancer Signaling and Translational Oncology (B.A., M.N., M.N.-P., L.B.L., S.E.G., H.S.P.), Biomedical Imaging (T.C., R.A.C., J.G.), and Pathology (H.K., S.L., L.R.), Genentech Inc., South San Francisco, California

Received May 6, 2016; accepted September 9, 2016

ABSTRACT

Glioblastoma multiforme (GBM) is the most common primary brain tumor in adults. Limited treatment options have only marginally impacted patient survival over the past decades. The phophatidylinositol 3-kinase (PI3K) pathway, frequently altered in GBM, represents a potential target for the treatment of this glioma. 5-(6,6-Dimethyl-4-morpholino-8,9-dihydro-6H-[1,4]oxazino[4,3-e] purin-2-yl)pyrimidin-2-amine (GDC-0084) is a PI3K inhibitor that was specifically optimized to cross the blood-brain barrier. The goals of our studies were to characterize the brain distribution, pharmacodynamic (PD) effect, and efficacy of GDC-0084 in orthotopic xenograft models of GBM. GDC-0084 was tested in vitro to assess its sensitivity to the efflux transporters P-glycoprotein (P-gp) and breast cancer resistance protein (BCRP) and in vivo in mice to evaluate its effects on the PI3K pathway in intact brain. Mice bearing U87 or GS2 intracranial tumors were treated with GDC-0084 to assess its brain distribution by matrix-assisted laser desorption ionization (MALDI) imaging and measure its PD effects and efficacy in GBM orthotopic models. Studies in transfected cells indicated that GDC-0084 was not a substrate of P-gp or BCRP. GDC-0084 markedly inhibited the PI3K pathway in mouse brain, causing up to 90% suppression of the pAkt signal. MALDI imaging showed GDC-0084 distributed evenly in brain and intracranial U87 and GS2 tumors. GDC-0084 achieved significant tumor growth inhibition of 70% and 40% against the U87 and GS2 orthotopic models, respectively. GDC-0084 distribution throughout the brain and intracranial tumors led to potent inhibition of the PI3K pathway. Its efficacy in orthotopic models of GBM suggests that it could be effective in the treatment of GBM. GDC-0084 is currently in phase I clinical trials.

Introduction

Glioblastoma multiforme (GBM) is the most frequently diagnosed primary brain tumor in adults, with more than 10,000 patients affected each year in the United States (Ostrom et al., 2015). Characterized by its invasiveness and aggressive progression, GBM, once diagnosed, presents a median survival of less than 2 years (Adamson et al., 2009). Treatment options have remained limited with few advances or successes in the past decades (Levin et al., 2015), and despite an aggressive standard therapy that includes surgery, radiation, and temozolomide, with the recent addition of bevacizumab at recurrence (Stupp et al., 2005; Friedman et al., 2009; Kreisl et al., 2009), only 5% of patients survive longer than 5 years. Molecular as well as regional and microenvironmental heterogeneity of GBM can be invoked to explain this lack of improvement (Phillips et al., 2006; Cloughesy et al., 2014). However, often overlooked is the significant challenge represented by the blood-brain barrier (BBB), constituted by tightly joined endothelial cells and efflux transporters such as P-glycoprotein (P-gp) and breast cancer resistance protein (BCRP) (de Vries et al., 2006). These transporters further reduce the permeability and delivery of drugs to the brain and prevent them from reaching therapeutic concentrations. While disruption of the BBB often occurs in GBM (Oberoi et al., 2016), and delivery of drugs to the tumor core has been shown (Hofer and Frei, 2007; Holdhoff et al., 2010), infiltrative regions of the tumor present an intact BBB and can only be reached by drugs able to cross the BBB and bypass efflux transporters.

Recent reports by the TCGA Research Network (Brennan et al., 2013) have identified major signaling pathways dysregulated in GBM. Among those, the phophatidylinositol 3-kinase (PI3K) pathway emerged as one of the most frequently altered, with mutation, amplification, or loss of key signaling proteins such as EGFR, PTEN, or PI3K, detected in more than 80% of GBM. Thus, this pathway represents a compelling target for the treatment of high-grade glioma. However, most, if not all, drugs acting on the PI3K pathway that have been tested, and have achieved disappointing results (Agarwal et al., 2011b), are substrates of P-gp and/or BCRP, the

dx.doi.org/10.1124/dmd.116.071423.

ABBREVIATIONS: A-B, apical to basolateral; B-A, basolateral to apical; BBB, blood-brain barrier; BCRP, breast cancer resistance protein; GBM, glioblastoma multiforme; GDC-0084, 5-(6,6-dimethyl-4-morpholino-8,9-dihydro-6H-[1,4]oxazino[4,3-e]purin-2-yl)pyrimidin-2-amine; LC-MS/MS, liquid chromatography–tandem mass spectrometry; MALDI, matrix-assisted laser desorption ionization; MDCK, Madin-Darby canine kidney; micro-CT, microcomputed tomography; Metoprolol, (RS)-1-(Isopropylamino)-3-[4-(2-methoxyethyl)phenoxy]propan-2-ol; MRI, magnetic resonance imaging; P_{app}, apparent permeability; pictilisib, 2-(1*H*-Indazol-4-yl)-6-(4-methanesulfonyl-piperazin-1-ylmethyl)-4-morpholin-4-yl-thieno[3,2-*d*]pyrimidine; PI3K, phophatidylinositol 3-kinase; *m/z*, mass-to-charge ratio; P-gp, P-glycoprotein.

two main efflux transporters expressed at the BBB. It is then expected that these compounds, including erlotinib (de Vries et al., 2012), everolimus (Chu et al., 2009), gefitinib (Agarwal et al., 2010), and lapatinib (Polli et al., 2009), will not be able to cross the BBB and are unlikely to maintain uniform and adequate concentrations throughout the brain.

5-(6,6-Dimethyl-4-morpholino-8,9-dihydro-6H-[1,4]oxazino[4,3-e]-purin-2-yl)pyrimidin-2-amine (GDC-0084) (Fig. 1A) is a selective inhibitor of PI3K (p110α K_i 2 nM) also able to potently inhibit mTOR (K_i 70 nM) (Heffron et al., 2016). This compound, possessing physicochemical properties optimized for brain penetration, was specifically developed as a potential treatment of GBM and is currently being evaluated in phase I in patients with high-grade glioma. GDC-0084 was shown to inhibit the proliferation of several glioma cells in vitro with IC_{50} ranging from 0.3 to 1.1 μM [U87: 0.74 μM (Heffron et al., 2016); GS2: 0.61 μM (unpublished data)]. In addition, this compound was also able to inhibit the phosphorylation of Akt in U87 human glioma implanted as a subcutaneous xenograft in nude mice, leading to significant tumor growth inhibition (Heffron et al., 2016).

The goals of the studies presented here were to characterize the PI3K pathway modulation and the efficacy of GDC-0084 in orthotopic models of human GBM and to investigate the brain and tumor distribution of GDC-0084 in these intracranial tumor models.

Materials and Methods

Chemicals

All Genentech compounds (> 99% pure), including GDC-0084, [D6]GDC-0084, and pictilisib [2-(1*H*-Indazol-4-yl)-6-(4-methanesulfonyl-piperazin-1-ylmethyl)-4-morpholin-4-yl-thieno[3,2-*d*]pyrimidine], were synthesized by Genentech, Inc. (South San Francisco, CA). All solvents used in analytical assays were purchased from Thermo Fisher Scientific (Watham, MA) and were of analytical or high-performance liquid chromatography grade. All other chemicals and reagents were purchased from Sigma-Aldrich (St. Louis, MO) unless otherwise specified.

In Vitro Studies

Transport Assays in Cell Monolayers. Madin-Darby canine kidney (MDCK) cells expressing human P-gp, human BCRP, or mouse Bcrp1 and LLC-PK1 cells transfected with mouse P-gp (mdr1a) were used to determine whether GDC-0084 was a substrate of these transporters. MDR1-MDCKI cells were licensed from the National Cancer Institute (Bethesda, MD) and Bcrp1-MDCKII, BCRP-MDCKII, and Mdr1a-LLC-PK1 cells were obtained from the Netherlands Cancer Institute (Amsterdam). For transport studies, cells were seeded on 24-well Millicell plates (Millipore, Billerca, MA) 4 days prior to use (polyethylene terephtalate membrane, 1 μm pore size) at a seeding density of 2.5×10^5 cells/ml (except for MDR1-MDCKI, which was seeded at a seeding density of 1.3×10^5 cells/ml). GDC-0084 was tested at 5 μM in the apical-to-basolateral (A-B) and basolateral-to-apical (B-A) directions. The compound was dissolved in transport buffer consisting of Hanks' balanced salt solution with 10 mM HEPES (Invitrogen Corporation, Grand Island, NY). Lucifer Yellow (Sigma-Aldrich) was used as the paracellular and monolayer integrity marker. GDC-0084 concentrations in the donor and receiving compartments were determined by liquid chromatography–tandem mass spectrometry (LC-MS/MS) analysis. The apparent permeability (P_{app}), in the apical to A-B and B-A directions, was calculated after 2-hour incubation as

$$P_{app}\left(10^{-6}\ \mathrm{cm/s}\right) = (dQ/dt) \cdot (1/AC_0)$$

where dQ/dt is the rate of compound appearance in the receiver compartment (fmol/s); A is the surface area of the insert (cm^2); and C_0 is the initial substrate concentration at T_0 (μM);The efflux ratio was calculated as ($P_{app,\ B\text{-}A}/P_{app,\ A\text{-}B}$).

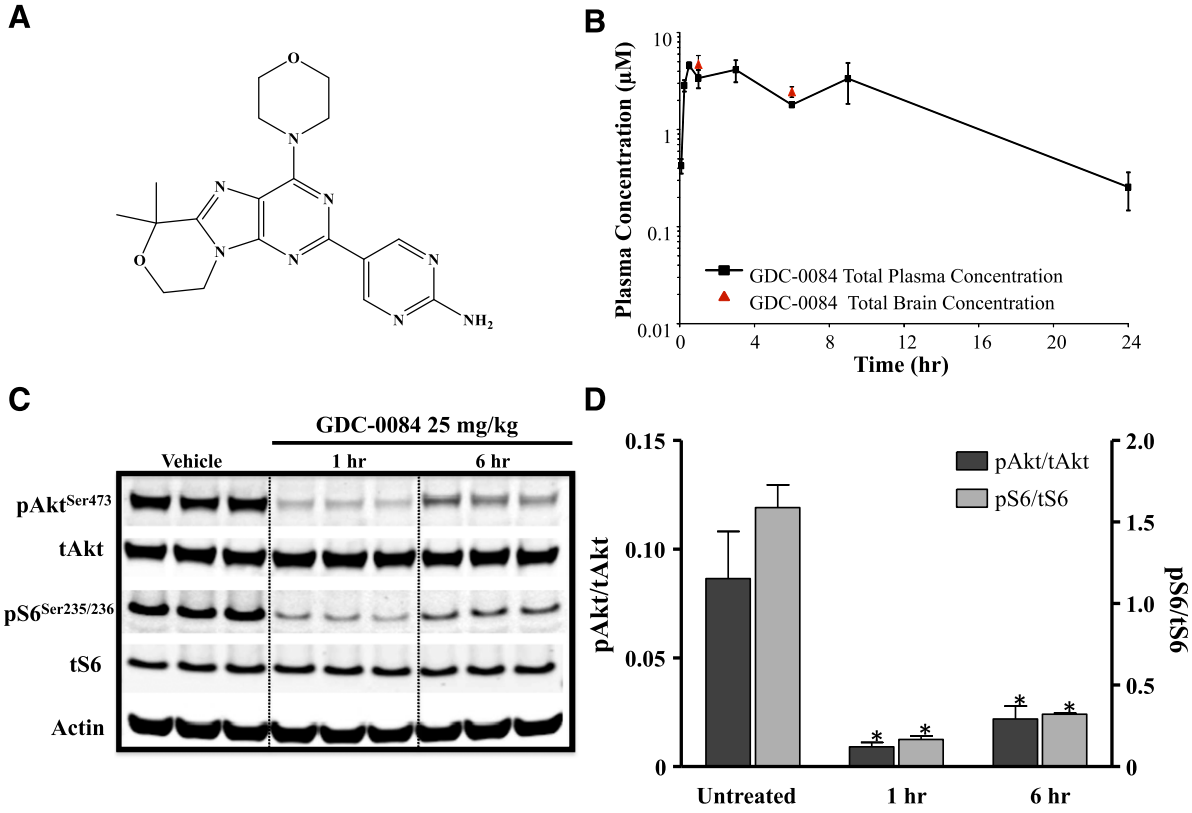

Fig. 1. (A) Chemical structure of GDC-0084. (B) Plasma concentration-time profile and brain concentrations of GDC-0084 following PO administration (25 mg/kg) to CD-1 mice. (C) Western blot of mouse brains probed with antibodies against pAkt, total Akt, pS6, total S6, and actin. (D) Quantitation of pAkt/total Akt and pS6/total S6 at 1 and 6 hours postdose in CD-1 mice. (B and D) Results are presented as the mean ± S.D. of three animals. * Significantly different from control. $P < 0.05$, t test.

Determination of Plasma Protein and Brain Binding. GDC-0084 protein binding was determined in vitro, in mouse plasma (Bioreclamation, Inc., Hicksville, NY) by equilibrium dialysis using a rapid equilibrium dialysis device (Thermo Scientific, Rockford, IL) as described previously (Salphati et al., 2012). Incubations were performed in triplicate. Parameters are presented as mean ± S.D. The binding of GDC-0084 to mouse brain was determined as described by Kalvass et al. (2007). Brain tissue was prepared and dialyzed as described previously (Salphati et al., 2012). Following dialysis, tissues and buffer samples were analyzed as outlined for the plasma protein binding studies.

In vivo Studies

All studies performed were approved by the Institutional Animal Care and Use Committee at Genentech, Inc. (South San Francisco, CA) and are described in Table 1.

Pharmacokinetic Study in Mouse. Female CD-1 mice (Charles River Laboratories, Hollister, CA) received a 25 mg/kg by mouth (PO) dose of GDC-0084 in 0.5% methylcellulose/0.2% Tween 80. Two blood samples (0.15 ml each) were collected from three mice per time point by retro-orbital bleed or terminal cardiac puncture while the animals were anesthetized with isoflurane. Blood samples were collected (with K_2EDTA as anticoagulant) predose and at 0.083, 0.25, 0.5, 1, 3, 6, 9, and 24 hours postdose. Samples were centrifuged within 1 hour of collection and plasma was separated and stored at −80°C until analysis. Total concentrations of GDC-0084 were determined by a nonvalidated LC-MS/MS assay. Back-calculated concentrations of the calibration curve (accuracy of calibration standards) were within 20% of the theoretical values. The linearity of the calibration curve was assessed and deemed acceptable if R^2 was greater than 0.98. Following plasma protein precipitation with acetonitrile, the supernatant was injected onto the column, a Phenomenex Kinetex C18 column (Phenomenex, Torrance, CA) (50 × 2 mm, 2.6 μm particle size). A CTC HTS PAL autosampler (LEAP Technologies, Chapel Hill, NC) linked to Thermo Scientific Accela UPLC pumps, coupled with an AB Sciex API 5500 Qtrap mass spectrometer (AB Sciex, Foster City, CA) were used for the LC-MS/MS assay. The aqueous mobile phase was water with 0.1% formic acid and the organic mobile phase was acetonitrile with 0.1% formic acid. The lower and upper limits of quantitation of the assay were 1 ng/ml and 20,000 ng/ml, respectively. The total run time was 1.5 minutes and the ionization was conducted in the positive ion mode. Brains were collected at 1 and 6 hour postdose from three different animals at each time point, rinsed with ice-cold saline, weighed, and stored at −80°C until analysis. For GDC-0084 quantitation, mouse brains were homogenized in 3 volumes of water. The homogenates were extracted by protein precipitation with acetonitrile. LC-MS/MS analysis was conducted as described for the plasma. The lower and upper limits of quantitation of the brain homogenate assay were 5 ng/ml and 11,000 ng/ml, respectively. Brain homogenate concentrations were converted to brain concentrations for the calculations of brain-to-plasma ratios.

Modulation of pAkt and pS6 in Brain. Female CD-1 mice were dosed PO with GDC-0084 at 25 mg/kg. Brains and plasma were collected at 1 and 6 hours postdose, from three animals at each time point. Each brain was split in half for pharmacodynamic analysis and GDC-0084 concentration measurement. The samples were stored at −80°C and analyzed for GDC-0084 total concentration. For pharmacodynamic analysis, cell extraction buffer (Invitrogen, Camarillo, CA) containing 10 mM Tris pH 7.4, 100 mM NaCl, 1 mM EDTA, 1 mM EGTA, 1 mM NaF, 20 mM $Na_4P_2O_7$, 2 mM Na_3VO_4, 1% Triton X-100, 10% glycerol, 0.1% SDS, and 0.5% deoxycholate was supplemented with phosphatase, protease inhibitors (Sigma, St. Louis, MO), and 1mM phenylmethylsulfonyl fluoride and added to frozen brain biopsies. Brains were homogenized, sonicated on ice, and centrifuged at 20,000*g* for 20 minutes at 4°C. Protein concentration was determined using BCA protein assay (Pierce, Rockford, IL). Proteins were separated by electrophoresis and transferred to NuPage nitrocellulose membranes (Invitrogen). A Licor Odyssey Infrared detection system (Licor, Lincoln, NE) was used to assess and quantify protein expression. PI3K pathway markers were evaluated by immunoblotting using antibodies against $pAkt^{Ser473}$, total Akt, $pS6^{Ser235/236}$, and total S6 (Cell Signaling Technologies, Danvers, MA). These antibodies cross react between human and mouse proteins, allowing detection of pathway markers in mouse brain as well as in the intracranially implanted human tumors. The differences in marker levels between the treated and control mice were evaluated using the Student's t-test (Prism 5, GraphPad, San Diego, CA).

Brain and Tumor Distribution by Matrix-Assisted Laser Desorption Ionization (MALDI) Imaging. Six female CD-1 nude mice (Charles River Laboratories) were implanted with either the U-87 MG/M (U87) glioblastoma cancer cells [a Genentech variant of U-87 MG cells from American Type Culture Collection (Manassas, VA)] or GS2 tumor cells (Günther et al., 2008), injected via stereotactic surgery into the right striatum in a volume of 3–5 μl (250 K U87 cells and 100 K GS2 cells). A single oral dose of 15 mg/kg GDC-0084 was administered 19–21 days postimplantation. The formulation was 0.5% methylcellulose/0.2% Tween 80. Mice were euthanized at 1 and 6 hours postdose via exsanguination by perfusion under anesthesia. Brains were excised, flash frozen in liquid N_2, and stored in a −80°C freezer until analyzed. Fresh-frozen tissue sections were obtained on a cryomicrotome (Leica CM3050S, Buffalo Grove, IL) at 12 μm thickness and thaw-mounted onto indium tin oxide–coated glass slides (Bruker Daltonics, Billerica, MA). Tissue sections were analyzed by imaging MALDI mass spectrometry, providing signal intensities (and not absolute quantitation), followed by cresyl violet staining for histologic interrogation.

Imaging MALDI Mass Spectrometry. A 40 mg/ml solution of 2,5-dihydroxybenzoic acid (Sigma-Aldrich) was prepared in methanol:water (70:30 v/v). A stable-labeled internal standard, [D6]GDC-0084, was spiked into the MALDI matrix solution at 2 μM prior to deposition onto the tissue sections. Matrix solution was homogenously spray-coated onto the tissue using a HTX TM-Sprayer (HTX technologies, Chapel Hill, NC). Matrix-coated tissue sections were transferred to the MALDI mass spectrometer (SolariX 7T FT-ICR, Bruker Daltonics, Bremen, Germany) for imaging analysis. Imaging data were collected at 100 μm pixel resolution in positive ionization mode, under continuous accumulation of selected ions windows optimized for a 50-Da window centered on mass-to-charge ratio (*m/z*) 383 (*m/z* 358–408). Laser intensity and number of shots were optimized for sensitivity of the parent drug (1200 shots) with ion detection collected over the mass range of *m/z* 150–3000. Drug images were generated based on accurate mass of the parent drug (GDC-0084 *m/z* 383.1938) using FlexImaging v4.0 64-bit (Bruker Daltonics, Billerica, MA) with a mass tolerance of ± 2 mDa and normalized to internal standard response.

Histology. Following completion of the imaging experiments, matrix coating was removed by rinsing the glass slide in 100% methanol for 30 seconds or until the entire matrix was visibly removed. Tissue sections were stained utilizing a freshly prepared 0.5% cresyl violet staining solution (Chaurand et al., 2004) by submerging the glass slide for 30 seconds, and then rinsed for an additional 30 seconds in two cycles of 100% ethanol. Microscope images were obtained on

TABLE 1

Study designs, experimental conditions, and measured endpoints for the in vivo studies

Study	Dose	Formulation	Mouse Strain	Collected Samples	Measured Endpoints
	mg/kg				
Pharmacokinetics	25	MCT	CD1, female	Plasma, brain	GDC-0084 concentrations PD modulation (pAkt, pS6)
MALDI imaging	15	MCT	CD-1 Nude, female intracranial tumor-bearing	Brain	GDC-0084 brain distribution
Efficacy	15	MCT	CD-1 Nude, female intracranial tumor-bearing	Plasma, brain, tumors	Tumor volumes GS2 tumors: GDC-0084 plasma, brain and tumor concentrations, PD modulation

MCT, 0.5% methylcellulose/0.2% Tween 80; PD, pharmacodynamic.

an Olympus BX51 (Tokyo) at 10× magnification and stitched using MicroSuite Analytical version 3.0 software (Olympus). Subsequently, stained images were coregistered to the optical images in FlexImaging for visualization and annotation of tumor and nontumor regions for the drug images.

Intratumor and Healthy Brain Distribution. To assess drug distribution, imaging MALDI mass spectrometry data from the U87 and GS2 tumor models were coregistered to the cresyl violet–stained microscope images in FlexImaging (Bruker Daltonics, Billerica, MA). Regions of interest were selected based on the anatomic features defined in the histologic image, including tumor and nontumor regions. Drug intensity for each pixel within the defined region of interest was extracted and exported. Drug intensities were binned in 0.1 increments over a range of 0.0–2.0. Histogram plots were created in GraphPad Prism 5 to visualize the distribution of pixel intensity frequencies.

Efficacy Studies in Brain Tumor Models. The U-87 MG/M (U87) glioblastoma cancer cells (a Genentech variant of U-87 MG cells from American Type Culture Collection) and the GS 2 (GS2) glioblastoma cells (Günther et al., 2008) were selected to test the efficacy of GDC-0084. These two models are PTEN-deficient, with the GS2 cell line having a copy number loss at the PTEN locus (Günther et al., 2008), and no detectable PTEN protein by western blot (Carlson et al., 2011). This glioblastoma stem-like (GS) cell line, derived from an adult patient, long-term survivor who had been subjected to two surgeries, radiation, and chemotherapy, presents mutations in the TP53 gene, no amplification of the EGFR gene, and formed spheres that grow semiadherently in vitro (Günther et al., 2008). The identity of the two cell lines was confirmed by short tandem repeat profiling (DNA Diagnostics Center, Fairfield, OH) using cells within five passages of those used for in vivo studies. The U87 (250 K) and GS2 (100 K) tumor cells were injected via stereotaxic surgery into the right striatum in a volume of 3–5 μl. For each experiment, mice were randomized into groups of 10 to obtain comparable mean tumor volumes between treatment and control groups for each model. Treatments were initiated at a time that ensured that the BBB had recovered from surgical disruption and tumors were expanding. Previous studies performed in our laboratories in intracranial models (and including sham surgery) indicated that the BBB had recovered from the disruption caused by the surgery after 7 days. Mice bearing intracranial U87 or GS2 xenografts were administered GDC-0084 (15 mg/kg), or vehicle (0.5% methylcellulose/0.2% Tween 80) PO daily for 2 or 4 weeks, respectively, starting 7 days (U87) or 14 days (GS2) post tumor cell inoculation. Mouse body weights were recorded twice per week during the study and animals were euthanized if body weight loss was greater than 20% from their initial body weight. Tumor volumes were monitored by ex vivo microcomputed tomography (micro-CT) imaging and T2 magnetic resonance imaging (MRI) for the GBM models U87 (on day 14 of dosing) and GS2 (predose and on day 28 of dosing), respectively. The differences between treatment groups were evaluated using Student's *t* test in Prism (GraphPad). MRI was performed on a Varian 9.4T MRI system with a 30-mm quadrature volume coil. During the imaging, animals were kept under anesthesia with 2% isoflurane in air. Body temperature was continuously monitored using a rectal probe and was maintained at 37°C by a heated-airflow system regulated by in-house LabVIEW controller software (National Instruments, Austin, TX). A T2-weighted fast spin echo, multi-slice sequence was used to detect lesions by MRI. Next, 12–20 axial 0.5–0.8-mm-thick slices were acquired with a 20 × 20 mm field of view, and 128 × 128 matrix, zero-filled to 256 × 256 images. Repetition time = 3500–4000 ms, echo time = 9–10 ms, echo train length = 8, k-zero = 4, number of excitations = 8. Tumor volumes were calculated from the T2-weighted fast spin echo, multi-slice images using an intensity threshold–based region-growing tool in MRVision software (MRVision, Co. Winchester MA). Brain sample preparation, micro-CT scanning, and image analysis for ex vivo micro-CT imaging were performed as described previously (de Crespigny et al., 2008).

In the studies conducted with the GS2 tumor-bearing mice, plasma and brains were also collected at the end of treatment to measure GDC-0084 concentrations and assess PI3K pathway modulation in the tumor. Each brain was dissected to separate the tumor from the healthy tissues. Plasma and normal brains were processed and analyzed by LC-MS/MS. The GS2 tumors isolated from the brains were processed and the PI3K pathway markers pAkt, pS6, and p4EBP1 were measured as described previously.

The effects of GDC-0084 on the PI3K pathway in GS2 orthotopic tumors were also evaluated by immunohistochemistry following the last PO dose of GDC-0084 (15 mg/kg) to mice after the 4-week treatment. Brains were collected 2 hours following the last dose, after the animals had been anesthetized with pentobarbital, perfused first with heparinized phosphate-buffered saline and subsequently with 4% paraformaldehyde.

Immunohistochemistry for detection of pAkt and pPRAS40 with antibodies D9E and C77D7, respectively (Cell Signaling Technologies), was performed on 4μ thick paraffin-embedded tissue sections using a Discovery XT autostainer and CC1 standard antigen retrieval (Ventana Medical Systems, Tucson, AZ). Specifically bound primary antibody was detected using OmniMap detection (Ventana Medical Systems) followed by hematoxylin counterstain. The antibodies used react with human and mouse proteins, allowing detection of pathway markers in mouse brain as well as in the intracranially implanted human tumors.

Results

In Vitro Studies

Transport Studies in Transfected Cell Lines. The permeability and bidirectional transport of GDC-0084 were measured in transfected cell lines overexpressing human or mouse P-gp or BCRP. The P_{app} value was high and comparable to that of (*RS*)-1-(Isopropylamino)-3-[4-(2-methoxyethyl)phenoxy]propan-2-ol (Metoprolol), the high P_{app} marker used in the same experiments (Table 2). The efflux ratios ($P_{app, B\text{-}A}/P_{app, A\text{-}B}$) did not markedly differ from 1 in the MDCK or LLC-PK1 transfected cells (Table 2), indicating that GDC-0084 was a poor substrate of these efflux transporters.

Plasma Protein and Brain Tissues Binding. GDC-0084 binding to plasma proteins was low, with a free fraction (%) of 29.5 ± 2.7 ($n = 3$) in CD-1 mouse plasma, when tested at 5 μM. Binding to brain tissues from CD-1 mice was higher, with a free fraction of 6.7% (± 1; $n = 3$).

In Vivo Studies

Pharmacokinetics of GDC-0084 in Mouse. The plasma concentration-time profile of GDC-0084 following a single oral dose (25 mg/kg) to mice is presented in Fig. 1B. Brain concentrations measured at 1 and 6 hours postdose were similar to plasma levels. Total and free brain-to-free plasma ratios of approximately 1.4 and 0.4, respectively, were consistent at the two time points (Table 3).

Modulation of pAkt and pS6 in Brain. Inhibition of the PI3K pathway was assessed in the brain of healthy mice through measurement of two markers, pAkt and pS6. Following a single oral dose of GDC-0084 (25 mg/kg), pAkt and pS6 levels were significantly lower than those detected in the control animals (Fig. 1C). Suppression of pAkt and pS6 reached 90% 1 hour postdose and stayed greater than 70% 6 hours after dosing (Fig. 1D).

Brain and Tumor Distribution by MALDI Imaging. Distribution of GDC-0084 in the brain and intracranial U87 and GS2 tumors following administration of a single PO dose (15 mg/kg) was investigated by MALDI imaging. Brains were collected 1 hour postdose

TABLE 2

Apparent permeability (P_{app}) of GDC-0084, Pictilisib, and Metoprolol in transfected cells

The results reported as mean ± S.D. (n = 4–6).

Compound	Cell Line	P_{app} (10^{-6} cm/s)		P_{app} Ratio B-A/A-B
		A-B	B-A	
GDC-0084	MDR1-MDCKI	13.5 ± 0.9	11.5 ± 1.6	0.85 ± 0.1
	Bcrp1-MDCKII	17.6 ± 2.1	18.6 ± 1.1	1.06 ± 0.1
	BCRP-MDCKII	23.2 ± 5.4	16.0 ± 1.1	0.71 ± 0.1
	Mdr1a-LLC-PK	13.1 ± 1.3	19.4 ± 1.3	1.48 ± 0.1
Pictilisib	MDR1-MDCKI	1.4 ± 0.2	37 ± 5.4	27 ± 0.2
	Bcrp1-MDCKII	0.47 ± 0.16	32 ± 3.2	80 ± 35
Metoprolol	MDR1-MDCKI	14.3 ± 4.9	13.4 ± 0.3	1.06 ± 0.4

Metoprolol, (*RS*)-1-(isopropylamino)-3-[4-(2-methoxyethyl)phenoxy]propan-2-ol.

TABLE 3

Plasma concentrations, brain concentrations and brain-to-plasma ratio of GDC-0084 following PO administration (25 mg/kg) to CD1 mice

The results are reported as mean ± S.D. (n = 3).

Time Postdose	Total			Free		
	Brain	Plasma	Brain-to-Plasma Ratio	Brain	Plasma	Brain-to-Plasma Ratio
hour	*μM*	*μM*		*μM*	*μM*	
1	4.72 ± 1.07	3.39 ± 0.72	1.39 ± 0.02	0.32 ± 0.07	0.76 ± 0.16	0.41 ± 0.01
6	2.46 ± 0.30	1.80 ± 0.09	1.37 ± 0.17	0.16 ± 0.02	0.41 ± 0.02	0.41 ± 0.05

and the images presented in Fig. 2 show that GDC-0084 distributed readily and quite evenly throughout the brain, including in the GS2 (Fig. 2A) and U87 (Fig. 2B) tumors. In addition, the homogeneity and pattern of distributions of GDC-0084 in the tumors and nontumor regions of the brains were further analyzed. To assess the homogeneity of the brain distribution in a more quantitative manner less prone to visual bias, the intensity of each pixel (signal) was extracted in the entire tumor region or in the whole nontumor, healthy area of the brains. The frequency of signal intensities (frequency of pixel intensities), binned by an increment of 0.1 as described in *Materials and Methods*, appeared to follow a normal distribution in healthy brain, superimposed (mean pixel intensity 0.54) to that observed in U87 tumors (Fig. 3A; mean pixel intensity 0.54). The similar mean pixel intensities in the two regions of the brain along with the superimposable Gaussian distributions indicated that the compound was able to reach the tumor and the nondiseased brain to a similar extent. A Gaussian distribution of signals was observed as well in GS2 tumors (Fig. 3B), also indicating a homogeneous tumor penetration; however, with a slightly lower mean pixel intensity (0.34 versus 0.55), suggesting an overall lower GDC-0084 concentration in GS2 tumors than in normal brain. Comparisons of the GDC-0084 signal homogeneity in nontumor brain regions between the U87 and GS2 tumor-bearing mice showed identical distribution (Fig. 3C) and mean pixel intensities, confirming the reproducible and consistent brain penetration properties of GDC-0084. Similar results were obtained in brains collected at 6 hours postdose. Furthermore, to contrast the distribution of GDC-0084 to that of a nonbrain penetrant compound, MALDI images previously obtained with pictilisib in the U87 tumor model (Salphati et al., 2014) were reanalyzed by extracting pixel intensity frequencies as described here. While signal intensities in the U87 tumor for GDC-0084 could be fit to a Gaussian curve, signals from pictilisib were concentrated in the low-intensity bins, with a distribution that appeared more heterogeneous (Fig. 3D). This can be interpreted as poor brain penetration due to leaky BBB, with localized hot spots of signal.

Efficacy in Brain Tumor Models. The efficacy of GDC-0084 was tested in the U87 and GS2 intracranial models. GDC-0084 was administered PO at 15 mg/kg daily for 2 and 4 weeks to U87 and GS2 tumor-bearing mice, respectively. The effect of the treatment on the U87 and GS2 tumor volumes was assessed at the end of the dosing period. Images of U87 tumor obtained by micro-CT are presented in Fig. 4A. The U87 tumor volumes were reduced by approximately 70% when

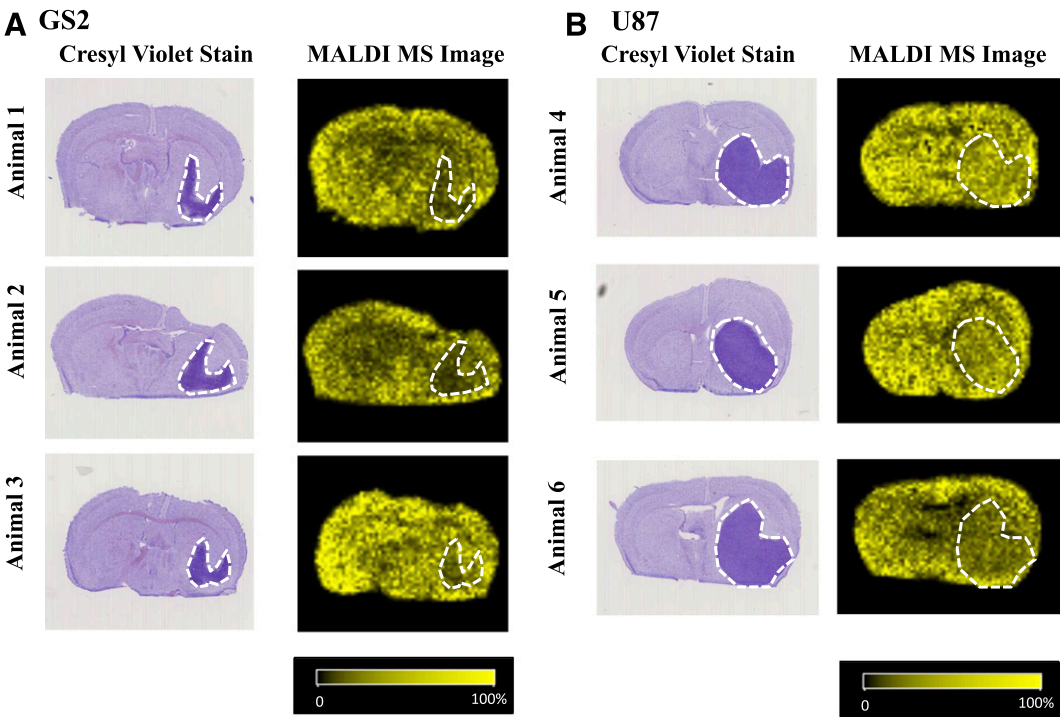

Fig. 2. Brain distribution of GDC-0084 in orthotopic models of GBM by MALDI imaging. Distribution of GDC-0084 in GS2 (A) and U87 (B) intracranial tumors 1 hour following PO administration of 15 mg/kg. Localizations of the tumors by cresyl violet staining and drug distribution in MALDI mass spectrometry (MS) images are presented. Dotted contours delineate the tumors.

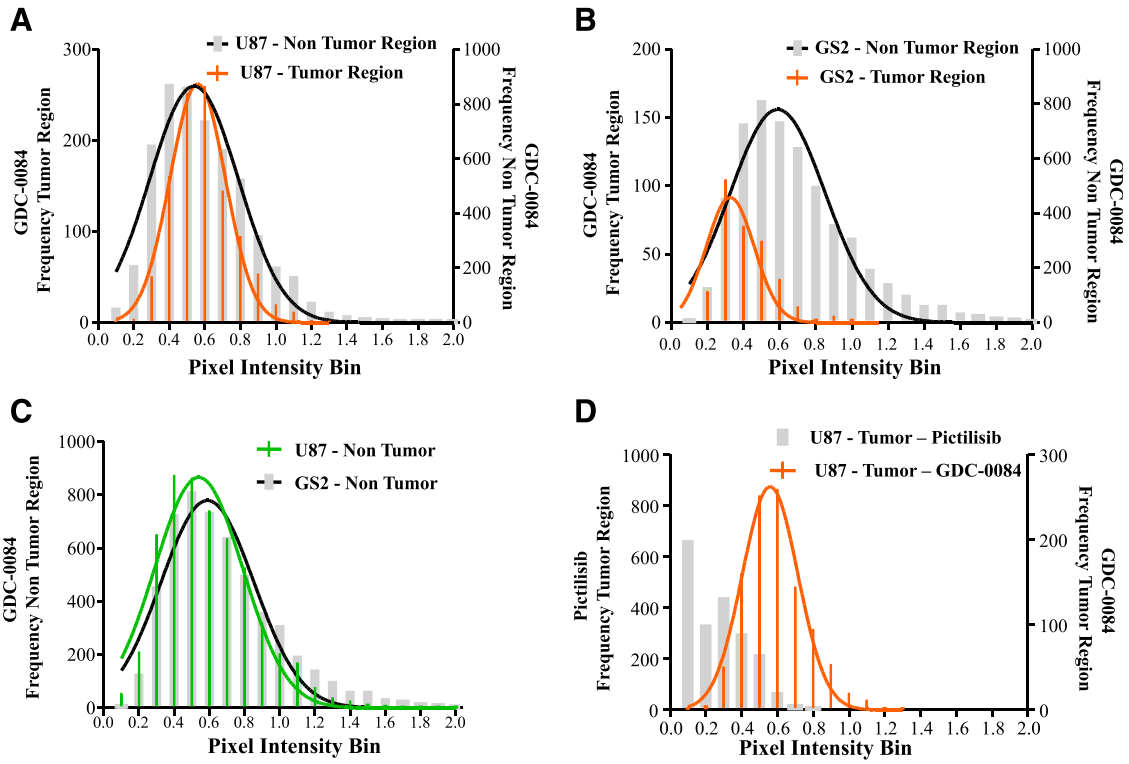

Fig. 3. Distribution of MALDI imaging signal intensity of GDC-0084 in U87 and GS2 intracranial tumors. (A) Distributions of signal intensity of GDC-0084 in tumor (orange bars) and nontumor regions (gray bars) in the U87 orthotopic GBM model. (B) Distributions of signal intensity of GDC-0084 in tumor (orange bars) and nontumor regions (gray bars) in the GS2 orthotopic GBM model. (C) Distributions of signal intensity of GDC-0084 in the nontumor regions of the U87 (green bars) and GS2 (gray bars) orthotopic GBM models. (D) Distributions of signal intensity of GDC-0084 (orange bars) and pictilisib (gray bars) in the U87 orthotopic GBM model. When appropriate, a Gaussian distribution curve was fitted to the signal intensity data.

compared with the vehicle control (Fig. 4B) following treatment with GDC-0084. Similarly, the GS2 tumors measured by MRI (Fig. 4C) in the treated mice were significantly ($P < 0.01$) smaller (≈40%) than those in the control group (Fig. 4D). Plasma and healthy brain concentrations of GDC-0084 were measured at the end of the study in the GS2 tumor-bearing mice and are presented along with brain-to-plasma ratios in Table 4. Brain concentrations in the normal part of the brain and brain-to-plasma ratios were comparable to those obtained previously (Table 3). Modulation of the PI3K pathway in the GS2 tumors was assessed by western blot at the end of the dosing period, 2 and 8 hours after the final administration of GDC-0084 (Fig. 5A). Levels of pAkt were significantly reduced at 2 and 8 hours, by 90% and 70%, respectively. Suppression of

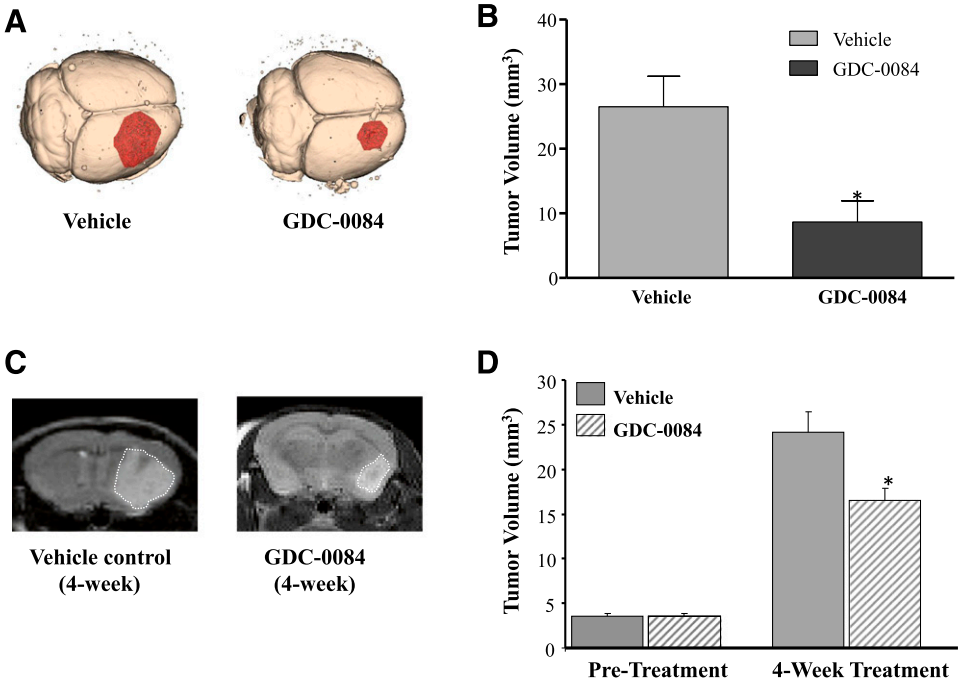

Fig. 4. Efficacy in orthotopic models of GBM. (A) Efficacy of GDC-0084 in U87 glioblastoma tumor model following treatment of 2 weeks. Representative micro-CT images of brain from control and treated mice. (B) U87 brain tumor volume in control mice and mice treated with GDC-0084 for 2 weeks. Results are presented as the mean ± S.E. of 10 animals. (C) Efficacy of GDC-0084 in GS2 neurosphere tumor model following treatment of 4 weeks. Representative T2-weighted MRI images of brain from control and treated mice. (D) GS2 brain tumor volume in control mice and mice treated with GDC-0084 for 4 weeks. Results are presented as the mean ± S.E. of 10 animals.

TABLE 4

Plasma concentrations, brain concentrations and brain-to-plasma ratio measured 2 and 8 hours following PO administration of GDC-0084 (15 mg/kg) to GS2 tumor-bearing mice (nontumor half of the brain)

The results are reported as mean ± S.D. (n = 3).

Time Postdose	Total			Free		
	Brain	Plasma	Brain-to-Plasma Ratio	Brain	Plasma	Brain-to-Plasma Ratio
hour	*μM*	*μM*		*μM*	*μM*	
2	5.51 ± 1.58	3.64 ± 2.05	1.67 ± 0.51	0.37 ± 0.11	1.07 ± 0.61	0.38 ± 0.11
8	2.48 ± 1.25	2.01 ± 1.19	1.29 ± 0.16	0.17 ± 0.08	0.59 ± 0.35	0.29 ± 0.03

pS6 and p4EBP1 was less pronounced at 2 hours, reaching 35% and 43%, respectively. These two markers were back to baseline levels 8 hours postdose (Fig. 5B). In addition, inhibition of the PI3K pathway was also measured at tumor cell level by immunohistochemistry. The tissue was probed with antibodies against the PI3K pathway markers pAkt and pPRAS40. GDC-0084 caused a marked reduction in staining when compared with the vehicle-treated animal (Fig. 5C), confirming inhibition of the pathway in the tumor.

Discussion

The PI3K pathway is altered in more than 80% of patients diagnosed with GBM. However, repeated failures of PI3K inhibitors in clinical trials may call into question the validity of this target or the ability to reach it for therapeutic benefit (Nichol and Mellinghoff, 2015).

To ensure delivery of the drug to its target and address one of the obstacles to effective treatment, the PI3K inhibitor GDC-0084 was specifically optimized to cross the BBB, while maintaining adequate potency (p110α K_i 2 nM; mTOR K_i 70 nM) and selectivity (Heffron et al., 2016) with the treatment of GBM and PI3K-dependent brain tumors as the primary objective. In vitro studies in MDCK and LLC-PK cells overexpressing human or mouse P-gp or BCRP indicated that GDC-0084 was not a good substrate of these two efflux transporters (Table 2), which limit the brain penetration of many compounds (Agarwal et al., 2011a). These in vitro results suggesting that GDC-0084 brain penetration would not be hindered by these transporters were consistent with data obtained in vivo in mice showing that GDC-0084 was able to cross the BBB following PO administration (25 mg/kg), and reach free brain concentrations greater than pAkt inhibition IC_{50} estimated in PC3 cells (0.13 μM; PTEN-null cells used in our program to test and select PI3K inhibitors) (Heffron et al., 2016). These levels of free drug (i.e., available to interact with the PI3K) at the target site (brain) achieved significant pathway suppression up to 6 hours postdose (Fig. 1). The total brain-to-plasma ratio exceeded 1 and the ratio of free concentrations in brain and plasma was 0.4 (Table 3). For drug passively permeating the BBB, the equilibrium theory of free drug applies (Tillement et al., 1988), and the ratio of unbound concentrations in the brain and plasma ($C_{u,br}/C_{u,p}$) is expected to equal (or approach) 1. Such ratios have been reported for the central nervous system drugs fluoxetine (0.41), citalopram (0.52), and caffeine (0.71) (Liu et al., 2006, 2014). For GDC-084, efflux transporters other than P-gp and BCRP may explain the lower $C_{u,br}/C_{u,p}$. Alternatively, experimental variability in the determination of the free fraction in brain and/or plasma may also have led to underestimation of this ratio. The in vitro determination of binding to brain homogenate has nevertheless been shown to be a reliable method to estimate free brain concentration (Liu et al., 2009). Despite this uncertainty, further analyses by MALDI imaging confirmed that GDC-0084 was able to distribute uniformly throughout the brain and tumors in the two orthotopic models of GBM tested (Fig. 2), the U87 and GS2 glioma cells. The U87 cell line is a widely used and characterized glioma model (Clark et al., 2010) that

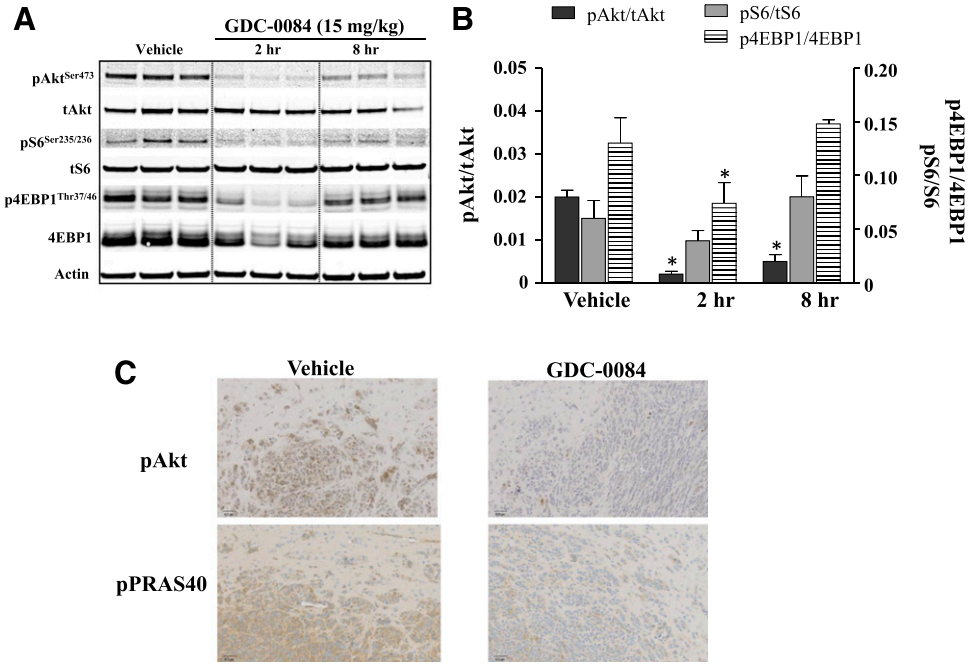

Fig. 5. Modulation of PI3K pathway in intracranial GS2 xenograft by GDC-0084. (A) Western blot of the PI3K pathway markers pAkt, pS6, and p4EBP1 in intracranial GS2 xenografts after completion of the 4-week efficacy dosing period. (B) Quantitation of pAkt/total Akt, p4EBP1/total 4EBP1, and pS6/total S6 at 2 and 8 hours following the last PO dose of GDC-0084 (15 mg/kg). (C) Immunohistochemical analysis of GS2 tumor-bearing brain section from vehicle-treated mice and mice dosed with GDC-0084 (15 mg/kg). Sections were probed for the PI3K markers pAkt and pPRAS40.

grows adherently when cultured and forms well-delineated tumors when implanted as intracranial xenograft. The GS2 cells grow in vitro as neurospheres and develop more diffusive tumors in the brain (Günther et al., 2008). While these two models present striking differences in their BBB status (intact versus disrupted) (Salphati et al., 2014), the analysis of drug signal intensity revealed a Gaussian distribution, reflective of homogeneous penetration of GDC-0084 in the U87 and GS2 tumors as well as in nontumor regions of the brain (Fig. 3), independent of the local variations in BBB integrity. In addition, in the U87 tumor model, mean pixel intensities (related to compound concentration) were similar in the tumor and in the healthy part of the brain, suggesting undifferentiated distribution in these two areas (Fig. 3A). In the GS2 tumors, signal intensities also appeared to follow a normal distribution, consistent with homogeneous penetration of the compound. The mean pixel intensity was nevertheless slightly lower in the tumor than in the nontumor region (0.37 versus 0.55). This weaker signal in the GS2 tumor may be caused by lower tumor vascularization, which could limit the diffusion of GDC-0084. The nearly superimposed frequencies of signal intensities in the healthy brain region of mice bearing either GS2 or U87 tumors underscore the consistency and reproducibility of GDC-0084 brain penetration (Fig. 3C). In contrast, reanalysis of data previously obtained with the P-gp and BCRP substrate (efflux ratios of 27 and 80, respectively) (Table 2) and nonbrain penetrant compound pictilisib (Salphati et al., 2014) showed heterogeneous (non-Gaussian) intratumor distribution of pixel intensities (Fig. 3D), most likely dependent on BBB disruption within the tumor, skewed toward low signal intensity (low levels of compound). Such a brain/tumor distribution is most likely representative of most of the unsuccessful targeted agents tested thus far against GBM. Homogeneous and undifferentiated compound distribution throughout healthy brain tissues and tumor is essential to potentially treat not only the core of the tumor but also invasive glioma cells protected by an intact BBB or blood-tumor barrier. Studies dissecting tumors and adjacent tissues from the rest of the brain in preclinical models have shown a sharp decrease in compound concentration from the tumor core, to the tumor rim, and to the normal brain with several targeted agents (Agarwal et al., 2012, 2013) that consequently failed to treat the whole brain. Such insufficient brain distribution in preclinical models of GBM is expected to mirror what occurs in patients with nonbrain penetrant drugs. Indeed, high concentrations of compounds, substrates of efflux transporters, have been measured in resected human brain tumors (Fine et al., 2006; Pitz et al., 2011), while these drugs had minimal therapeutic effects. Similarly, high levels of erlotinib were shown to colocalize with the contrast-enhancing regions of brain metastases (Weber et al., 2011).

The potent inhibition of the PI3K pathway in the brain, as well as the distribution in healthy tissues and brain tumor, suggested that GDC-0084 could be efficacious in orthotopic models of GBM. Studies in the U87 and GS2 models showed that GDC-0084 could significantly reduce tumor volumes, compared with the vehicle control. While promising, the findings in the U87 tumors were not unexpected since this model presents a disrupted BBB and can be sensitive to compounds with limited brain distribution (Carcaboso et al., 2010; Salphati et al., 2012). However, this GBM model may represent what might occur in the contrast-enhancing regions of a human GBM. The GS2 model, in contrast, possesses an intact BBB (Salphati et al., 2014) and recapitulates better the invasive regions of GBM. In that model, GDC-0084 administration significantly reduced tumor volume when compared with vehicle treatment and led to marked suppression of the PI3K pathway (Fig. 5), assessed by western blot and immunohistochemistry (Fig. 5C). However, this significant efficacy was less pronounced than in the U87 model, despite comparable in vitro potency against the two cell lines. This may be attributed to the slightly lower concentration of GDC-0084 in the GS2 tumor suggested by MALDI imaging, or could also indicate that pathways other than PI3K contribute to the growth of these tumors. This hypothesis may only be tested with the combination of agents able to cross the BBB and distribute throughout the brain, such as GDC-0084. When considering the genetic heterogeneity of GBM, such combination therapies may be necessary to achieve optimal efficacy.

Multiple studies and a recent symposium have emphasized the role of the BBB and efflux transporters (or blood-tumor barrier) in limiting the therapeutic effects of most targeted drugs evaluated in GBM clinical trials (Agarwal et al., 2011b; Levin et al., 2015; Oberoi et al., 2016). While it is not the only challenge, it still appears to be an underappreciated obstacle (Mason, 2015) to optimal GBM treatment. In addition, maintaining or improving potency against pathways or targets involved in GBM, as well as ensuring that adequate free concentrations are reached in the brain (Smith et al., 2010) are also key elements in the optimization of potential drugs. The PI3K inhibitor GDC-0084 was purposely designed to cross an intact BBB and distribute throughout the brain. It is being evaluated in patients, and exposures reached at tolerated doses are consistent with those associated with efficacious doses in mouse models. While brain penetrance is a necessary but not sufficient attribute, this compound may provide a much needed treatment option for GBM and should allow a more informative assessment of pharmacodynamic hypotheses.

Authorship Contributions

Participated in research design: Salphati, Alicke, Heffron, Shahidi-Latham, Nishimura, Pang, Quiason, Gould, Phillips, Olivero.

Conducted experiments: Alicke, Nishimura, Cheong, Lau, Lee, Plise.

Contributed new reagents or analytic tools: Shahidi-Latham, Cao, Carano, Greve, Quiason, Rangell, Zhang.

Performed data analysis: Salphati, Shahidi-Latham, Quiason, Cao, Nannini-Pepe, Pang, Phillips.

Wrote or contributed to the writing of the manuscript: Salphati, Shahidi-Latham, Carano, Koeppen.

References

Adamson C, Kanu OO, Mehta AI, Di C, Lin N, Mattox AK, and Bigner DD (2009) Glioblastoma multiforme: a review of where we have been and where we are going. *Expert Opin Investig Drugs* **18**:1061–1083.

Agarwal S, Hartz AM, Elmquist WF, and Bauer B (2011a) Breast cancer resistance protein and P-glycoprotein in brain cancer: two gatekeepers team up. *Curr Pharm Des* **17**:2793–2802.

Agarwal S, Manchanda P, Vogelbaum MA, Ohlfest JR, and Elmquist WF (2013) Function of the blood-brain barrier and restriction of drug delivery to invasive glioma cells: findings in an orthotopic rat xenograft model of glioma. *Drug Metab Dispos* **41**:33–39.

Agarwal S, Mittapalli RK, Zellmer DM, Gallardo JL, Donelson R, Seiler C, Decker SA, Santacruz KS, Pokorny JL, Sarkaria JN, et al. (2012) Active efflux of Dasatinib from the brain limits efficacy against murine glioblastoma: broad implications for the clinical use of molecularly targeted agents. *Mol Cancer Ther* **11**:2183–2192.

Agarwal S, Sane R, Gallardo JL, Ohlfest JR, and Elmquist WF (2010) Distribution of gefitinib to the brain is limited by P-glycoprotein (ABCB1) and breast cancer resistance protein (ABCG2)-mediated active efflux. *J Pharmacol Exp Ther* **334**:147–155.

Agarwal S, Sane R, Oberoi R, Ohlfest JR, and Elmquist WF (2011b) Delivery of molecularly targeted therapy to malignant glioma, a disease of the whole brain. *Expert Rev Mol Med* **13**: e17.

Brennan CW, Verhaak RG, McKenna A, Campos B, Noushmehr H, Salama SR, Zheng S, Chakravarty D, Sanborn JZ, Berman SH, et al.; TCGA Research Network (2013) The somatic genomic landscape of glioblastoma. *Cell* **155**:462–477.

Carcaboso AM, Elmeliegy MA, Shen J, Juel SJ, Zhang ZM, Calabrese C, Tracey L, Waters CM, and Stewart CF (2010) Tyrosine kinase inhibitor gefitinib enhances topotecan penetration of gliomas. *Cancer Res* **70**:4499–4508.

Carlson BL, Pokorny JL, Schroeder MA, and Sarkaria JN (2011) Establishment, maintenance and in vitro and in vivo applications of primary human glioblastoma multiforme (GBM) xenograft models for translational biology studies and drug discovery. *Curr Protoc Pharmacol* **14**:1–14.

Chaurand P, Schwartz SA, Billheimer D, Xu BJ, Crecelius A, and Caprioli RM (2004) Integrating histology and imaging mass spectrometry. *Anal Chem* **76**:1145–1155.

Chu C, Abbara C, Noël-Hudson MS, Thomas-Bourgneuf L, Gonin P, Farinotti R, and Bonhomme-Faivre L (2009) Disposition of everolimus in mdr1a−/1b− mice and after a pre-treatment of lapatinib in Swiss mice. *Biochem Pharmacol* **77**:1629–1634.

Clark MJ, Homer N, O'Connor BD, Chen Z, Eskin A, Lee H, Merriman B, and Nelson SF (2010) U87MG decoded: the genomic sequence of a cytogenetically aberrant human cancer cell line. *PLoS Genet* **6**: e1000832.

Cloughesy TF, Cavenee WK, and Mischel PS (2014) Glioblastoma: from molecular pathology to targeted treatment. *Annu Rev Pathol* **9**:1–25.

de Crespigny A, Bou-Reslan H, Nishimura MC, Phillips H, Carano RA, and D'Arceuil HE (2008) 3D micro-CT imaging of the postmortem brain. *J Neurosci Methods* **171**:207–213.

de Vries NA, Beijnen JH, Boogerd W, and van Tellingen O (2006) Blood-brain barrier and chemotherapeutic treatment of brain tumors. *Expert Rev Neurother* **6**:1199–1209.

de Vries NA, Buckle T, Zhao J, Beijnen JH, Schellens JH, and van Tellingen O (2012) Restricted brain penetration of the tyrosine kinase inhibitor erlotinib due to the drug transporters P-gp and BCRP. *Invest New Drugs* **30**:443–449.

Fine RL, Chen J, Balmaceda C, Bruce JN, Huang M, Desai M, Sisti MB, McKhann GM, Goodman RR, Bertino JS, Jr, et al. (2006) Randomized study of paclitaxel and tamoxifen deposition into human brain tumors: implications for the treatment of metastatic brain tumors. *Clin Cancer Res* **12**:5770–5776.

Friedman HS, Prados MD, Wen PY, Mikkelsen T, Schiff D, Abrey LE, Yung WK, Paleologos N, Nicholas MK, Jensen R, et al. (2009) Bevacizumab alone and in combination with irinotecan in recurrent glioblastoma. *J Clin Oncol* **27**:4733–4740.

Günther HS, Schmidt NO, Phillips HS, Kemming D, Kharbanda S, Soriano R, Modrusan Z, Meissner H, Westphal M, and Lamszus K (2008) Glioblastoma-derived stem cell-enriched cultures form distinct subgroups according to molecular and phenotypic criteria. *Oncogene* **27**: 2897–2909.

Heffron TP, Ndubaku CO, Salphati L, Alicke B, Cheong J, Drobnick J, Edgar K, Gould SE, Lee LB, Lesnick JD, et al. (2016) Discovery of clinical development candidate GDC-0084, a brain penetrant inhibitor of PI3K and mTOR. *ACS Med Chem Lett* **7**:351–356.

Hofer S and Frei K (2007) Gefitinib concentrations in human glioblastoma tissue. *J Neurooncol* **82**: 175–176.

Holdhoff M, Supko JG, Gallia GL, Hann CL, Bonekamp D, Ye X, Cao B, Olivi A, and Grossman SA (2010) Intratumoral concentrations of imatinib after oral administration in patients with glioblastoma multiforme. *J Neurooncol* **97**:241–245.

Kalvass JC, Maurer TS, and Pollack GM (2007) Use of plasma and brain unbound fractions to assess the extent of brain distribution of 34 drugs: comparison of unbound concentration ratios to in vivo P-glycoprotein efflux ratios. *Drug Metab Dispos* **35**:660–666.

Kreisl TN, Kim L, Moore K, Duic P, Royce C, Stroud I, Garren N, Mackey M, Butman JA, Camphausen K, et al. (2009) Phase II trial of single-agent bevacizumab followed by bevacizumab plus irinotecan at tumor progression in recurrent glioblastoma. *J Clin Oncol* **27**: 740–745.

Levin VA, Tonge PJ, Gallo JM, Birtwistle MR, Dar AC, Iavarone A, Paddison PJ, Heffron TP, Elmquist WF, Lachowicz JE, et al. (2015) CNS anticancer drug discovery and development conference white paper. *Neuro-oncol* **17** (Suppl 6):vi1–vi26.

Liu X, Cheong J, Ding X, and Deshmukh G (2014) Use of cassette dosing approach to examine the effects of P-glycoprotein on the brain and cerebrospinal fluid concentrations in wild-type and P-glycoprotein knockout rats. *Drug Metab Dispos* **42**:482–491.

Liu X, Smith BJ, Chen C, Callegari E, Becker SL, Chen X, Cianfrogna J, Doran AC, Doran SD, Gibbs JP, et al. (2006) Evaluation of cerebrospinal fluid concentration and plasma free concentration as a surrogate measurement for brain free concentration. *Drug Metab Dispos* **34**: 1443–1447.

Liu X, Van Natta K, Yeo H, Vilenski O, Weller PE, Worboys PD, and Monshouwer M (2009) Unbound drug concentration in brain homogenate and cerebral spinal fluid at steady state as a surrogate for unbound concentration in brain interstitial fluid. *Drug Metab Dispos* **37**: 787–793.

Mason WP (2015) Blood-brain barrier-associated efflux transporters: a significant but underappreciated obstacle to drug development in glioblastoma. *Neuro-oncol* **17**:1181–1182.

Nichol D and Mellinghoff IK (2015) PI3K pathway inhibition in GBM—is there a signal? *Neuro-oncol* **17**:1183–1184.

Oberoi RK, Parrish KE, Sio TT, Mittapalli RK, Elmquist WF, and Sarkaria JN (2016) Strategies to improve delivery of anticancer drugs across the blood-brain barrier to treat glioblastoma. *Neuro Oncol* **18**:27–36.

Ostrom QT, Gittleman H, Fulop J, Liu M, Blanda R, Kromer C, Wolinsky Y, Kruchko C, and Barnholtz-Sloan JS (2015) CBTRUS statistical report: primary brain and central nervous system tumors diagnosed in the United States in 2008–2012. *Neuro Oncol* **17** (Suppl 4): iv1–iv62.

Phillips HS, Kharbanda S, Chen R, Forrest WF, Soriano RH, Wu TD, Misra A, Nigro JM, Colman H, Soroceanu L, et al. (2006) Molecular subclasses of high-grade glioma predict prognosis, delineate a pattern of disease progression, and resemble stages in neurogenesis. *Cancer Cell* **9**:157–173.

Pitz MW, Desai A, Grossman SA, and Blakeley JO (2011) Tissue concentration of systemically administered antineoplastic agents in human brain tumors. *J Neurooncol* **104**:629–638.

Polli JW, Olson KL, Chism JP, John-Williams LS, Yeager RL, Woodard SM, Otto V, Castellino S, and Demby VE (2009) An unexpected synergist role of P-glycoprotein and breast cancer resistance protein on the central nervous system penetration of the tyrosine kinase inhibitor lapatinib (*N*-3-chloro-4-[(3-fluorobenzyl)oxy]phenyl-6-[5-([2-(methylsulfonyl)ethyl]aminomethyl)-2-furyl]-4-quinazolinamine; GW572016). *Drug Metab Dispos* **37**:439–442.

Salphati L, Heffron TP, Alicke B, Nishimura M, Barck K, Carano RA, Cheong J, Edgar KA, Greve J, Kharbanda S, et al. (2012) Targeting the PI3K pathway in the brain—efficacy of a PI3K inhibitor optimized to cross the blood-brain barrier. *Clin Cancer Res* **18**:6239–6248.

Salphati L, Shahidi-Latham S, Quiason C, Barck K, Nishimura M, Alicke B, Pang J, Carano RA, Olivero AG, and Phillips HS (2014) Distribution of the phosphatidylinositol 3-kinase inhibitors Pictilisib (GDC-0941) and GNE-317 in U87 and GS2 intracranial glioblastoma models-assessment by matrix-assisted laser desorption ionization imaging. *Drug Metab Dispos* **42**:1110–1116.

Smith DA, Di L, and Kerns EH (2010) The effect of plasma protein binding on in vivo efficacy: misconceptions in drug discovery. *Nat Rev Drug Discov* **9**:929–939.

Stupp R, Mason WP, van den Bent MJ, Weller M, Fisher B, Taphoorn MJ, Belanger K, Brandes AA, Marosi C, Bogdahn U, et al.; European Organisation for Research and Treatment of Cancer Brain Tumor and Radiotherapy Groups; ; National Cancer Institute of Canada Clinical Trials Group (2005) Radiotherapy plus concomitant and adjuvant temozolomide for glioblastoma. *N Engl J Med* **352**:987–996.

Tillement JP, Urien S, Chaumet-Riffaud P, Riant P, Bree F, Morin D, Albengres E, and Barre J (1988) Blood binding and tissue uptake of drugs. Recent advances and perspectives. *Fundam Clin Pharmacol* **2**:223–238.

Weber B, Winterdahl M, Memon A, Sorensen BS, Keiding S, Sorensen L, Nexo E, and Meldgaard P (2011) Erlotinib accumulation in brain metastases from non-small cell lung cancer: visualization by positron emission tomography in a patient harboring a mutation in the epidermal growth factor receptor. *J Thorac Oncol* **6**:1287–1289.

Address correspondence to: Dr. Laurent Salphati, Genentech, Inc., 1 DNA Way, South San Francisco, CA 94080. E-mail: salphati.laurent@gene.com